Ceramics International 46 (2020) 19996–20003

Contents lists available at ScienceDirect

Ceramics International

journal homepage: www.elsevier.com/locate/ceramint

Crystal structure, Raman spectra and microwave dielectric properties of novel temperature-stable $LiYbSiO_4$ ceramics

Congxue Su[a,b,*], Laiyuan Ao[c], Zhiwei Zhang[a], Yifan Zhai[a], Junqi Chen[a], Ying Tang[a,b], Laijun Liu[a,b], Liang Fang[a,b,c,**]

[a] Guangxi Universities Key Laboratory of Non-ferrous Metal Oxide Electronic Functional Materials and Devices, College of Material Science and Engineering, Guilin University of Technology, Guilin, 541004, China
[b] Guangxi Universities Key Laboratory of Optical and Electronic Materials and Devices, Guilin University of Technology, Guilin, 541004, China
[c] College of Materials and Chemical Engineering, Key Laboratory of Inorganic Nonmetallic Crystalline and Energy Conversion Materials, China Three Gorges University, Yichang, 443002, China

ARTICLE INFO

Keywords:
$LiYbSiO_4$
Raman spectra
Microwave dielectric properties
Structure

ABSTRACT

Olivine – type structure microwave dielectric ceramics $LiYbSiO_4$ with near-zero τ_f were fabricated by solid-state reaction process for the first time. The relationships among structural parameters, sintering behavior, vibrational modes and microwave dielectric properties for the ceramics were studied. The variation in ε_r could be correlated with Raman shift. The variation in $Q\times f$ values was inversely correlated to FWMH and average cation covalency. The τ_f values were explained with the bond valence sum of cations. Single phase $LiYbSiO_4$ ceramics could be obtained at the range of 1100–1140 °C and showed promising microwave dielectric properties with ε_r = 7.36 – 7.42, $Q\times f$ = 19081 – 25276 GHz and τ_f = +4.52 – +8.03 ppm/°C.

1. Introduction

In the past decades, microwave (MW) communications experienced an exponential growth in terms of a great deal of users and applications. Due to the rapid growth of communication system, 4G technology could not provide greater capacity and faster signal response performance, thus pushing the technology upgrade from 4G to 5G rapidly [1–3]. On account of low latency (time delay), large bandwidths, and high-speed data transfer are the main characteristics of 5G technology, new microwave dielectric materials with low ε_r and high $Q\times f$ need to be further explored. More importantly, near-zero τ_f is critical to ensure operating stability of the device [4].

In order to in search of novel high-performance materials for 5G applications, much attentions have been attracted on the silicates owing to the fact that the Si–O bond in [SiO_4] tetrahedrons could restrict the rattling cations and thus lead to the low ε_r and high $Q\times f$ [5]. Up to now, many kinds of Si-based microwave dielectrics with desirable properties have been reported. As summarized in Table 1 [6–24], downsides to practical applications are distinctly for many silicate ceramics because of their high densification temperatures (≥1300 °C) and large τ_f values ($|\pm\tau_f| \geq 10$ ppm/°C). However, it's worth noting that olivine-type Mg_2SiO_4 possessed an extremely high $Q\times f$ except the imperfection of high sintering temperature which was as high as 1450 °C [7]. On the other hand, $LiInSiO_4$ also adopts the olivine structure, but it could be well sintered at a comparatively low sintering temperature (1150 °C) among these ceramics listed in Table 1. Actually, olivine-type materials include not only some orthosilicates or germanates belonging to $X_2^{II}SiO_4$ ($X_2^{II}GeO_4$), but also exist in many other compounds, which may be derived from the Mg_2SiO_4 formula. For instance, 2 Mg^{II} could be substituted by $A^{I}B^{III}$, viz, $A^{I}B^{III}SiO_4$, and $Mg^{II}Si^{IV}$ could be replaced by $A^{I}C^{V}$, such as $A^{I}B^{II}C^{V}O_4$ (C^{V} = P, V or As) [25]. In recent years, Li-containing microwave ceramics with olivine-structure like $LiMPO_4$ (M = Mg, Ni and Mn) [26–29] and $LiYGeO_4$ [30] have drawn many attentions originated from their low sintering temperatures (< 1000 °C). But unfortunately, large negative τ_f for phosphates and expensive-cost material for germanates are still unpractical in commercialization.

Developing new Li-based silicates with satisfying performance in 5G microwave field seems to be more feasible and significant. Olivine structured $LiYbSiO_4$ with low conductivity was firstly reported by

* Corresponding author. Guangxi Universities Key laboratory of non-ferrous metal oxide electronic functional materials and devices, College of Material Science and Engineering, Guilin University of Technology, Guilin, 541004, China.
** Corresponding author. Guangxi Universities Key laboratory of non-ferrous metal oxide electronic functional materials and devices, College of Material Science and Engineering, Guilin University of Technology, Guilin, 541004, China.
E-mail addresses: alpes1987@163.com (C. Su), fanglianggl001@aliyun.com (L. Fang).

https://doi.org/10.1016/j.ceramint.2020.05.070
Received 2 April 2020; Received in revised form 5 May 2020; Accepted 6 May 2020
Available online 15 May 2020

Table 1
Microwave dielectric properties of some Si-based ceramics.

No	Silicate Ceramics	Crystal Structure	T (°C)	ε_r	$Q\times f$ (GHz)	τ_f (ppm/°C)	Ref
1	Li_2ZnSiO_4	Monoclinic Silicate	1250	5.8	14700	−96.6	[6]
2	Mg_2SiO_4	Orthorhombic Forstreite	1450	6.8	270000	−67	[7]
3	$CaMgSi_2O_6$	Monoclinic Pyroxene	1290	7.5	60000	−46	[8]
4	Zn_2SiO_4	Rhombohedral Willemite	1340	6.6	219000	−61	[9]
5	$Ca_3MgSi_2O_8$	Monoclinic Merwinite	1375	13.8	27000	−62	[10]
6	$LiInSiO_4$	Orthorhombic olivine	1150	8.2	12600	−55	[11]
7	Nd_2SiO_5	Monoclinic Silicate	1500	7.94	38800	−53	[12]
8	$BaAl_2Si_2O_8$	Monoclinic Paracelsian	1475	6.36	44800	−46.9	[13]
9	$CaSm_4Si_3O_{13}$	Hexagonal Apatite	1375	13.7	17700	−38.1	[14]
10	$Sr_2Al_2SiO_7$	Tetragonal Gehlenite	1525	7.2	33000	−37	[15]
11	$Mg_2Al_4Si_5O_{18}$	Orthorhombic Cordierite	1350	6.3	39000	−32	[16]
12	$BaY_2Si_3O_{10}$	Monoclinic Trisilicate	1400	9.5	65600	−28	[17]
13	Al_2SiO_5	Orthorhombic Sillimanite	1525	4.4	41800	−17	[18]
14	$SrTb_4Si_3O_{13}$	Hexagonal Apatite	1500	14.3	19300	6	[19]
15	$LiEu_9(SiO_4)_6O_2$ + 2 wt% LiF	Hexagonal Apatite	1250	14.1	7100	8	[20]
16	$LiAlSiO_4$	Hexagonal β-Eucryptite	1350	4.8	36000	8	[21]
17	$CaSnSiO_5$	Monoclinic Malayaite	1525	9.1	61000	35	[22]
18	$Ba_9Y_2Si_6O_{24}$	Trigonal Silicate	1400	14.9	22440	35.8	[23]
19	Li_2TiSiO_5	Tetragonal Natisite	1180	9.89	38100	50.1	[24]
20	$LiYbSiO_4$	Orthorhombic Olivine	1120	7.42	25276	4.52	this work

Nakayama et al., and it could be well calcined at 1000 °C [31]. Similar to $LiInSiO_4$, [YbO_6] octahedrons are corner shared and cross linked by [SiO_4] tetrahedrons, forming a three-dimensional (3D) network with Li channels along < 100 > directions. But lithium migration energy barrier of $LiYbSiO_4$ was slightly bigger than that of $LiInSiO_4$, which indicates that Li^+ conductivity and dielectric loss might be lower in $LiYbSiO_4$ [31–33]. Besides, it is notable that despite being promising cathode materials for lithium battery, some olivine-type $LiMPO_4$ still exhibited high $Q\times f$ values owning to the hopping carrier Li^+ had a contribution in dielectric relaxation, rather than in conductivity at microwave frequency [26,28]. In addition, [YbO_6] and [InO_6] octahedrons might play different roles in determining dielectric performance, such as Ba_2YbNbO_6 (τ_f = +2 ppm/°C) can offer advantage over Ba_2InNbO_6 (τ_f = +17 ppm/°C) especially in the thermal stability [34]. Considering the favorable information given above and the microwave dielectric properties of $LiYbSiO_4$ ceramics were not investigated up to now. Therefore, in the present work we initially report the microwave dielectric properties of $LiYbSiO_4$ ceramics, the structural parameters, sintering behavior, and Raman spectrum are also discussed in the paper.

2. Experimental procedure

$LiYbSiO_4$ ceramics were synthesized by a solid-phase reaction route using Li_2CO_3 (99.99%, Aladdin Biological Technology Co. Ltd., Shanghai, China), Yb_2O_3 (99.99%; Xilong Chemicals, Guangdong, China), and SiO_2 (99.99%, Guo-Yao Co, Ltd, Shanghai, China) as raw materials. Before weighting, Yb_2O_3 powders were calcined at 1000 °C for 1.5 h. Then the raw powders were weighed stoichiometrically and ball-milled in alcohol for 8 h. The obtained slurries were dried and calcined at 1000 °C for 2 h. The calcined samples were re-grounded in alcohol for 8 h. Then the powders were pressed into cylinders under a pressure of 100 MPa with 5 wt% PVA. To limit lithium evaporation during the sintering process, the samples were muffled with the same compositions and sintered at 1100–1140 °C for 6 h.

Phase composition of the sintered $LiYbSiO_4$ ceramics was studied by X-ray diffraction using Panalytical X'pert Pro diffractometer with Cu Kα radiation. Bulk densities of ceramics were measured through Archimedes method. Morphology of the sintered specimens was analyzed by using Hitachi S4800 scanning electron microscope. The Raman spectra were recorded at room temperature by using a Raman spectrometer (Thermo Fisher Scientific DXR, America) with a 532 nm line in the range of 100–1200 cm^{-1}. The microwave dielectric properties were measured by an Agilent N5230A network analyzer and a Delta 9039 oven. The τ_f value was calculated as follows:

$$\tau_f = \frac{f_{85} - f_{25}}{(85 - 25) \times f_{25}} \quad (1)$$

where, f_{85} and f_{25} are the resonant frequencies at 85 °C and 25 °C, respectively.

3. Results and discussion

Fig. 1 presents the X-Ray diffraction patterns of $LiYbSiO_4$ ceramics sintered at 1100–1140 °C for 6 h. All the diffraction peaks for sintered ceramics were assigned to the standard pattern of $LiTmSiO_4$ (JCPDS # 82–1449), indicating the pure orthorhombic olivine-type phase was formed in all ceramics. In order to investigate the variations of cell parameters of $LiYbSiO_4$ ceramics at great length, rietveld refinements of the XRD patterns were carried out by FullProf software based on a structural model of $LiTmSiO_4$. The corresponding refinement result is shown in Fig. 2(a–e) and Table 2. Obviously, in the range of 1100 °C–1120 °C, the unit-cell parameter increased gradually along with the sintering temperature, which resulted in the increase of unit-

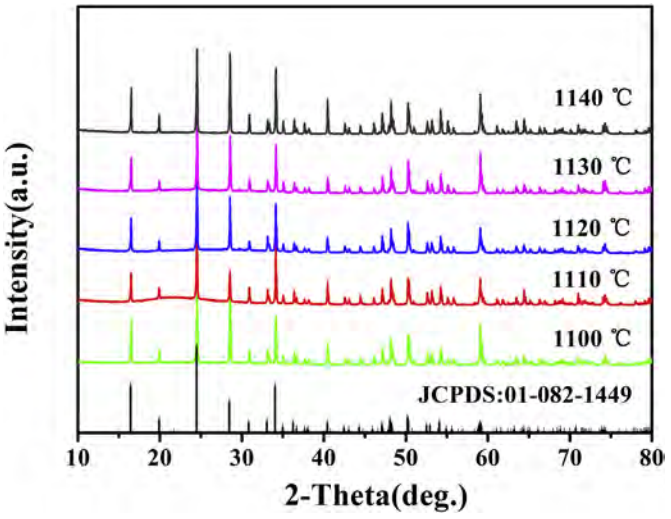

Fig. 1. X-Ray diffraction patterns of $LiYbSiO_4$ ceramics sintered at 1100–1140 °C for 6 h.

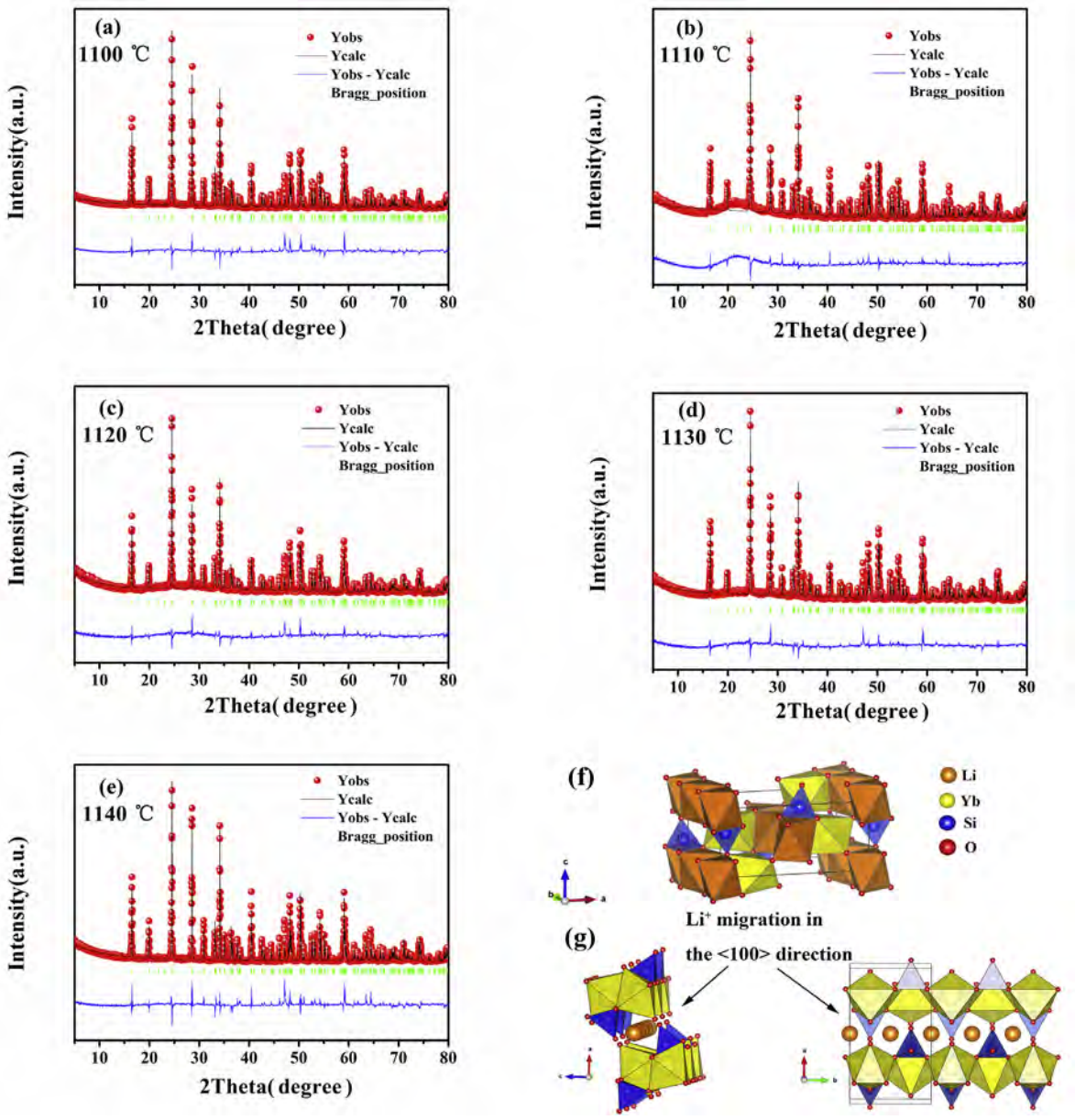

Fig. 2. Rietveld XRD patterns of $LiYbSiO_4$ ceramics sintered at different temperatures (a-e corresponding to 1100–1140 °C); (f) and (g) Schematic crystal structure of $LiYbSiO_4$ ceramic.

cell volume from 328.77 Å^3 to 328.92 Å^3. The reason for lattice expansion could be regarded as large particle sizes, and the major influence in the lattice parameters could be surface tension [35–37]. Further increase in temperature to 1140 °C, however, led to a decline in unit-cell to a value of 328.69 Å^3. It was reported that the cation vacancy caused lattice contraction, in other words, the volatilization of Li^+ at high sintering temperatures in our cases might give rise to the decrease in unit-cell [38]. Fig. 2f and g display the schematic representations of

Table 2
Refinement parameters and reliability of $LiYbSiO_4$ ceramics with different sintering temperatures.

Structural parameters	Sintering temperatures (°C)				
	1100	1110	1120	1130	1140
a (Å)	10.7447(2)	10.7451(2)	10.7469(3)	10.7447(3)	10.7431(2)
b (Å)	6.2481(3)	6.2486(2)	6.2488(1)	6.2487(2)	6.2478(2)
c (Å)	4.8972(1)	4.8974(1)	4.8978(1)	4.8971(1)	4.8970(1)
$\alpha = \beta = \gamma$ (°)	90	90	90	90	90
V (Å^3)	328.77(4)	328.82(3)	328.92(3)	328.80(4)	328.69(4)
R_p(%)	11.6	11.2	11.1	11.5	11.5
R_{wp}(%)	14.1	13.6	13.8	13.9	14.0
χ^2	2.13	1.91	1.99	2.09	2.07

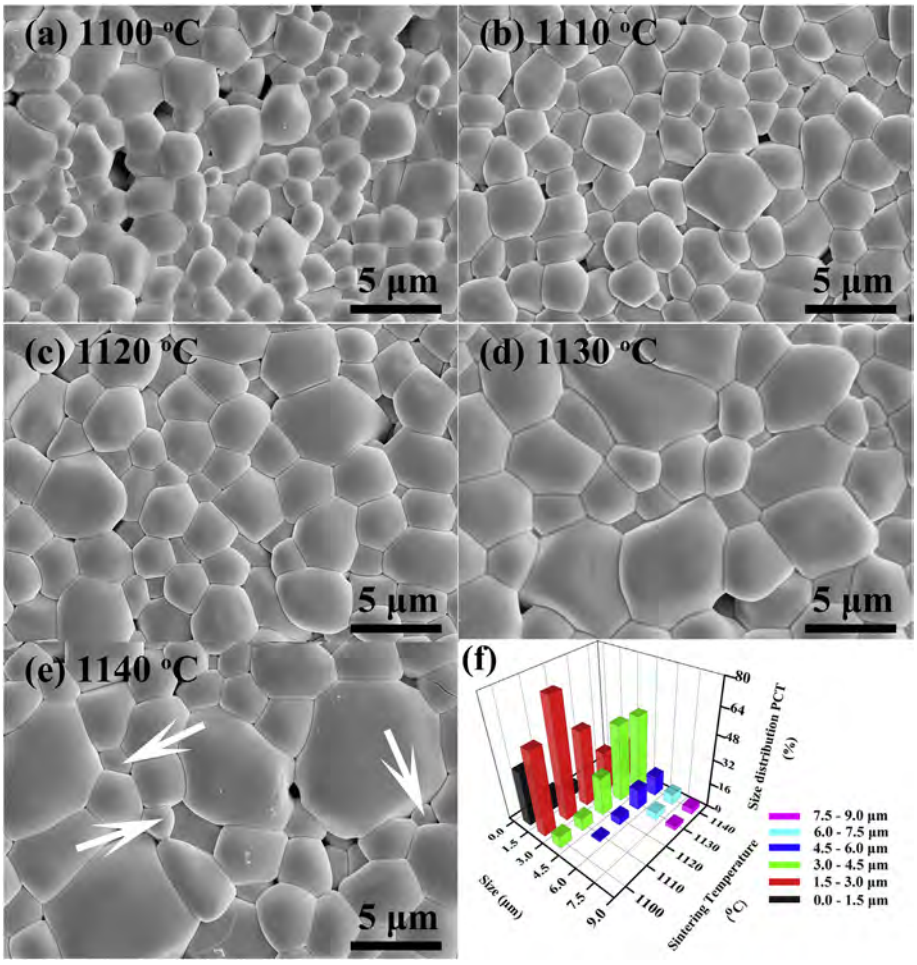

Fig. 3. SEM images of the $LiYbSiO_4$ ceramics sintered at different temperatures (a) 1100 °C, (b)1110 °C, (c) 1120 °C, (d) 1130 °C, (e) 1140 °C; (f) Variation of grain size and size distribution percentage with sintering temperatures in $LiYbSiO_4$ ceramics.

olivine-type $LiYbSiO_4$. In the structure, chains are composed of $[YbO_6]$ and $[LiO_6]$ octahedrons, each distorted $[YbO_6]$ octahedron is edge-sharing with two $[LiO_6]$ octahedrons, which are in turn edge sharing with other $[LiO_6]$ octahedra in the chain. On the other hand, each $[YbO_6]$ octahedron corner-sharing in the chain, and two neighbouring $[YbO_6]$ octahedrons are edge and corner sharing to a $[SiO_4]$ tetrahedron. The $[SiO_4]$ tetrahedra are isolated from each other and cross link with $[YbO_6]$ octahedrons, forming a 3D network with tunnels occupied by Li^+ along the [001] and [010] directions.

Fig. 3a-e show SEM images of $LiYbSiO_4$ ceramics sintered at 1100–1140 °C for 6 h and the grain size distribution of sintered ceramics are shown in Fig. 3f. For the ceramic sintered at 1100 °C, a porous microstructure was developed with many pores and the small grains were preponderant inside the ceramic. The grain size increased slightly and slight pores were observed at 1110 °C, and it can be found that the ceramic sintered at 1120 °C obtained the dense and uniform microstructure with clear grain boundaries. However, abnormal grain growth and degradation in grain uniformity began to appear at 1130 °C, and a few large grains (about 9 μm) together with several poles could be found intuitively in ceramic sintered at 1140 °C. It is noticeable that a few small grains could be observed at the grain boundaries in the ceramic sintered at 1140 °C, perhaps by reason of some abnormal grains impinged upon each other in the early stages of grain growth [39]. Similar to several Li-containing silicates [11,20,40], low density can be correlated with porosity observed in all $LiYbSiO_4$ ceramics. Variation of grain size and size distribution percentage with sintering temperatures in $LiYbSiO_4$ ceramics are exhibited in Fig. 3f. Small grains (< 1.5 μm) mainly occurred in the ceramic sintered below 1110 °C, larger and uniform grains were found in the ceramic sintered at 1120 °C, and oversintering (1130 and 1140 °C) would cause abnormal grain (7.5–9 μm) growth.

The Raman spectra of $LiYbSiO_4$ ceramics sintered at various temperatures is revealed in Fig. 4. The factor group analysis ($\boldsymbol{k} = 0$) of the

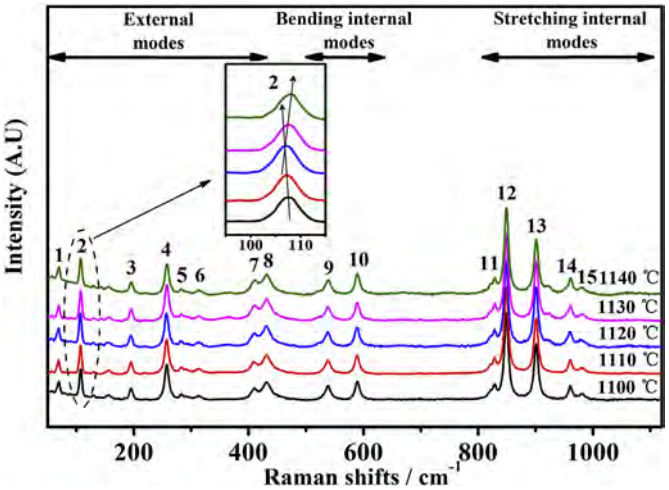

Fig. 4. Raman spectra of $LiYbSiO_4$ ceramics sintered at different temperatures; Magnified spectra of wavelength in the region of 95–115 cm^{-1}.

Table 3
The Raman active modes of experiment for $LiYbSiO_4$ ceramic sintered at 1140 °C and compared with data of literatures.

Band	Raman active modes (cm^{-1})		Symmetry modes	Assignments
	Observation	Literature		
1	70	72	A_g	Yb^{3+} translation mode
2	108	111	A_g	Yb^{3+} translation mode
3	196	199	A_g	Yb^{3+} translation mode
4	258	261	B_{2g}	SiO_4 and Yb^{3+} translation mode
5	283	287	B_{2g}	SiO_4 and Yb^{3+} translation mode
6	314	320	$B_{1g} + B_{3g}$	SiO_4 rotational mode
7	412	412	B_{3g}	ν_2 (SiO_4) (External mode)
8	432	437	$B_{1g} + B_{2g}$	$\nu_2 + \nu_2$ (External mode)
9	539	542.5	A_g	ν_4 (SiO_4) (Bending mode)
10	590	593	$B_{1g} + B_{2g} + B_{3g}$	$\nu_4 + \nu_4 + \nu_4$ (Bending mode)
11	829	827	A_g	$\nu_1 + \nu_3$ (Stretching internal mode)
12	849	851.5	A_g	ν_1 (SiO_4) (Stretching internal mode)
13	901	905	B_{3g}	ν_3 (SiO_4) (Stretching internal mode)
14	961	963	A_g	ν_3 (SiO_4) (Stretching internal mode)
15	981	983	B_{1g}	ν_3 (SiO_4) (Stretching internal mode)

olivine-structure shows 84 vibrational modes and they can be classified by the following set of irreducible representations: $\Gamma = 11A_g + 7B_{1g} + 11B_{2g} + 7B_{3g} + 10A_u + 14B_{1u} + 10B_{2u} + 14B_{3u}$. According to the symmetry selection rules, the total Raman-active modes of olivine are $11A_g + 7B_{1g} + 11B_{2g} + 7B_{3g}$. Due to the overlapped Raman vibration bands or the low resolution of instrument, the number of Raman frequencies observed in Fig. 4 is less than 36 Raman active modes in olivine. The Raman active modes and assignments of $LiYbSiO_4$ ceramic sintered at 1140 °C are listed in Table 3. As expounded in the previous studies of olivine-type silicates [25,41,42], the weak peaks below 350 cm^{-1} could be associated with the translational modes in which 70, 108 and 196 cm^{-1} were influenced by Yb^{3+}, and the mode 6 at 314 cm^{-1} was assigned to SiO_4 rotational mode. The peaks at the range of 400–440 cm^{-1} and 530–600 cm^{-1} were related to external modes and bending modes, respectively. The frequencies of 800–1000 cm^{-1} were attributed to the internal stretching vibrations of the [SiO_4] tetrahedra, and the modes 11–15 corresponding to $LiYbSiO_4$ were very closed to the reported in earlier literature [41]. Furthermore, the enlarged spectra of the Raman shift in the region of 95–115 cm^{-1} are also presented in Fig. 4. The Raman mode 2 firstly shifted toward low frequency and then shifted toward high frequency with the increasing temperature. The red shift might be attributed to a slight expansion in the [YbO_6] octahedron, while the blue shift could be explained by the shrinkage in the [YbO_6] octahedron. The variation tendency was consistent with the variation in cell volume (see Table 2). According to researches, bond strength had a strong relationship with Raman shift, the oxygen octahedron became rigid as bond strength increased, thus lead to the weaker damping behavior and the blue shift of Raman mode [43,44]. To calculate the bond strength of $LiYbSiO_4$ ceramics, the empirical expression was used [45]:

$$s = \left(\frac{R}{R_1}\right)^{-N_1} \tag{2}$$

where R is the refined bond length, R_1 and N_1 are the universal parameters. The refined bond lengths and corresponding bond strength are listed in Table 4 and Table 5, respectively. It can be seen that the variation in bond strength of Yb–O was strongly influenced by the average bond length (d_{ave}) of Yb–O, indicating the Raman shift of mode 2 were closely associated with the variation in the volume of [YbO_6] octahedron.

Variation of relative density, average grain size, Raman shift, FWMH, sum of cation bond valence, and microwave dielectric properties of $LiYbSiO_4$ ceramics are plotted in Fig. 5. From 1100 °C to 1120 °C, the relative density increased as the sintering temperature increased, reaching to a maximum value of 94.26% at 1120 °C, and then decreased to 91.92% at 1140 °C. At the same time, with the increase of sintering temperature, the trend of average grain size increased and coincided well with the microstructure. The variation tendency of ε_r was similar to that of relative density and higher density corresponded to higher ε_r. Hence, to eliminate the influence of porosity, the corrected ε_r can be corrected by the Bosman and Havinga's correction [46]:

Table 4
The refined bond length and average bond length of $LiYbSiO_4$ ceramics sintered at different sintering temperatures.

Type of bond length	Sintering temperatures (°C)				
	1100	1110	1120	1130	1140
Li–O (1) × 2	2.3468(8)	2.2975(9)	2.1702(9)	2.1643(9)	2.1457(7)
Li–O (2) × 2	2.2312(6)	2.1893(5)	2.1899(8)	2.1424(7)	2.1319(6)
Li–O (3) × 2	2.3657(11)	2.1774(7)	2.2318(4)	2.2619(12)	2.2609(12)
d_{ave}	2.3146	2.2214	2.1973	2.1895	2.1795
Yb–O (1)	2.1026(11)	2.2195(10)	2.1849(10)	2.2278(11)	2.2302(10)
Yb–O (2)	2.1085(5)	2.1120(4)	2.1421(5)	2.1801(5)	2.1821(5)
Yb–O (3) × 2	2.2513(10)	2.2682(7)	2.3104(9)	2.2915(9)	2.2885(9)
Yb–O (3) × 2	2.0837(7)	2.2762(4)	2.2509(6)	2.1207(6)	2.1085(5)
d_{ave}	2.1469	2.2367	2.2416	2.2054	2.2011
Si–O (1)	1.7512(8)	1.8173(5)	1.7920(7)	1.8641(7)	1.8019(7)
Si–O (2)	1.5831(10)	1.7409(8)	1.6511(7)	1.6193(9)	1.7810(8)
Si–O (3) × 2	1.6729(4)	1.5863(3)	1.6628(2)	1.6399(5)	1.5846(3)
d_{ave}	1.67	1.6827	1.6922	1.6908	1.688

$$\varepsilon_{corrected} = \varepsilon_m(1 + 1.5p) \tag{3}$$

where, $\varepsilon_{corrected}$ and ε_m are the corrected and measured ε_r, P is the fractional porosity. According to the equation, $LiYbSiO_4$ ceramic sintered at 1120 °C had the $\varepsilon_{corrected}$ of 8.06. In addition, the Clausius–Mossotti equation and additive rule were used to calculate the theoretical permittivity ε_{theo} [47,48]:

$$\varepsilon_{theo} = \frac{1 + 2b\alpha_{theo}/V_m}{1 - b\alpha_{theo}/V_m} \tag{4}$$

$$\alpha_{theo} = \alpha(Li^+) + \alpha(Yb^{3+}) + \alpha(Si^{4+}) + 4\alpha(O^{2-}) \tag{5}$$

where α_{theo}, b, and V_m represent the sum polarizability, $4\pi/3$, and molar volume, respectively. The calculated theoretical permittivity of $LiYbSiO_4$ ceramic sintered at 1120 °C is 7.90, which is very close to the measured value of 7.42. Furthermore, Raman spectroscopy is quiet sensitive to the crystal structure so as to investigate the association between lattice vibrations and microwave dielectric properties [43]. In our case, the Raman mode 2 was produced by the external vibration of Yb^{3+} against oxygen octahedron [40,44], the red shift of mode 2

Table 5
Distortion of octahedron, bond valence, bond strength, and covalence (f_c) of cations in $LiYbSiO_4$ ceramics, the average cation covalency, sum of cation bond valence, sum of cation bond strength, and the microwave dielectric properties of $LiYbSiO_4$ ceramics.

		Sintering temperatures (°C)				
		1100	1110	1120	1130	1140
[LiO6] octahedron	Δ_{octa} (%)	6.60×10^{-4}	5.92×10^{-4}	1.37×10^{-4}	5.63×10^{-4}	7.04×10^{-4}
	Bond valence (v.u)	0.6137	0.7870	0.8333	0.8571	0.8826
	Bond strength (v.u)	0.734	0.8664	0.9017	0.9186	0.9372
	f_c	0.3015	0.3912	0.4165	0.4288	0.4426
	Covalency %	41.08	45.15	46.19	46.68	47.23
[YbO6] octahedron	Δ_{octa} (%)	1.20×10^{-3}	0.70×10^{-3}	0.75×10^{-3}	1.04×10^{-3}	1.16×10^{-3}
	Bond valence (v.u)	3.9493	3.0808	3.0415	3.3684	3.4155
	Bond strength (v.u)	0.6582	0.5135	0.5069	0.5614	0.5693
	f_c	0.2541	0.1721	0.1686	0.1979	0.2023
	Covalency %	38.61	33.52	33.26	35.25	35.53
[SiO4] tetrahedron	Bond valence (v.u)	3.5782	3.5367	3.3652	3.4513	3.4973
	Bond strength (v.u)	3.5813	3.5526	3.3765	3.4658	3.5168
	f_c	3.6311	3.5855	3.3105	3.449	3.529
	Covalency %	101.39	100.93	98.05	99.52	100.35
Average cation covalency %		60.36	59.87	59.17	60.48	61.04
Cation bond valence sum (v.u)		8.1412	7.4045	7.24	7.6768	7.7954
Cation bond strength sum (v.u)		4.9735	4.9325	4.7851	4.9458	5.0233
ε_r		7.36	7.39	7.42	7.38	7.36
Q × f (GHz)		21177	23841	25276	22710	19081
τ_f (ppm/°C)		8.03	5.58	4.52	6.81	7.52

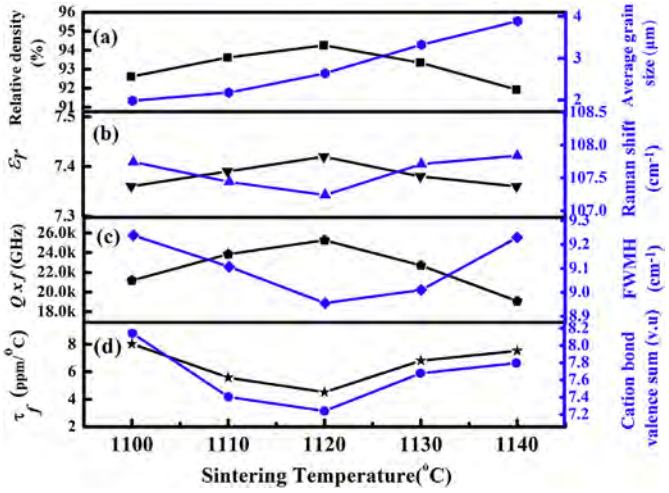

Fig. 5. Relative density and relationship between Raman shift, FWMH, average grain size, sum of cation bond valence and microwave dielectric properties of $LiYbSiO_4$ ceramics sintered at 1100–1140 °C for 6h.

revealed the increase in volume of oxygen octahedron, and that would exert influence on the polarization of Yb^{3+} in the [YbO_6] octahedron. Therefore, the relationship between ε_r and Raman shift could be explained as follows [49]:

$$\varepsilon_r(0,\ \xi,\ k) = \frac{\Omega_p^2 \exp[\lambda(E_F^o - \xi)]}{\omega(\xi,\ k)} \tag{6}$$

where ε_r, Ω_p, and ω are the dielectric constant, plasma frequency and phonon frequency, respectively. As shown in Fig. 5b, with increasing sintering temperature, the variation of ε_r was contrary to the Raman shift of mode 2, that is, the relationship between ε_r and Raman shift conformed to equation (6).

The relationship between $Q\times f$ values and FWHM is illustrated in Fig. 5c. Generally speaking, the FWHM of symmetric stretching vibrations in high frequencies (such as A_g peaks around 849 cm^{-1} in this work) was often used to correlate the $Q\times f$ [43,50]. It is clear that an inverse trend between FWHM of A_g mode (i.e., mode 12) and $Q\times f$ from 1100 °C to 1140 °C. The $LiYbSiO_4$ ceramic sintered at 1120 °C obtained a minimum FWMH value and a maximum $Q\times f$ value of 25276 GHz, implying a high degree of ordering and low phonon damping might be achieved, which in turn resulted in the higher $Q\times f$ value [50,51]. Externally, the increase of $Q\times f$ value in this work can be ascribed to the reduction of porosity and the average grain size. The small grains resulted in more grain boundaries and brought about the lattice mismatch with higher dielectric loss, while the large grains would worsen the grain uniformity and generate degradation of quality factor [52]. Internally, other structural parameters like bond valence and covalency are also closely related to the $Q\times f$ value [20]. The bond valence of the cation V_i can be calculated by Eqs. (7) and (8) [53]:

$$v_{ij} = exp\left[\frac{R_{ij} - d_{ij}}{b}\right] \tag{7}$$

$$V_{ij} = \sum v_{ij} \tag{8}$$

where v_{ij} is the bond valence, R_{ij} is the bond valence parameter, d_{ij} is the bond length between atom i and j, and b is the universal constant of 0.37 Å. The covalency f_c can be described by the empirical equations as follows [45]:

$$f_c = as^M \tag{9}$$

$$\text{Covalency } (\%) = \frac{f_c}{s} \times 100 \tag{10}$$

where a = 0.49 v.u., s is the bond length and M = 1.57. The bond valence, covalency f_c of cation-oxygen bonds, average cation covalency, sum of cation bond valence and the microwave dielectric dielectrics of $LiYbSiO_4$ ceramics are summarized in Table 5. Owing to a smaller sum of discrepancy factor, an inverse relationship between the cation covalency and quality factor has been revealed in some microwave dielectric ceramics, such as $LiRe_9(SiO_4)_6O_2$ (Re = La, Pr, Nd), $Ca_{1-x}Cd_xMoO_4$ (x = 0–1) and $Ba_3MM'_2O_9$ (M = Mg, Zn, Ni and M' = Ta and Nb) [20,53,54]. In the present study, a similar relationship existed also between the $Q\times f$ and the average cation covalency. Although the $Q\times f$ values of $LiYbSiO_4$ were higher than that of $LiInSiO_4$ [11], but it is worth noting that the dielectric loss of $LiYbSiO_4$ in microwave frequency were larger than that of some olivine structured $LiMPO_4$ [25,27]. Considering the sintering temperatures of silicates were much higher than that of phosphates in Li-based olivine, the volatilization of Li^+ might be more severe in $LiYbSiO_4$, namely, more Li^+ vacancy sites in Li channels would be generated, which could accelerate ionic

conductivity more easily and aggravate dielectric loss accordingly. Investigation about the effect of Li^+ motion on the microwave dielectric properties of $LiYbSiO_4$ ceramics will be carry out in the future work.

Some investigations reported that there was an association with τ_f and the distortion of the oxygen octahedron [20,55,56]. The distortion of octahedron in $LiYbSiO_4$ ceramics can be formulated as follows [56]:

$$\Delta_{octahedron} = \frac{1}{6}\sum\left[\frac{R_i - \bar{R}}{\bar{R}}\right]^2 \quad (11)$$

where R_i is the individual bond length, and $\bar{R}$ is the average bond length of the octahedron. The corresponding results of distortion listed in Table 5 also showed a similar tendency with the τ_f values, meaning the bond strength of polyhedral and degree of distortion in $LiYbSiO_4$ ceramics have strong effects on τ_f. According to earlier reports, τ_f was also strongly dependent on the bond valences of ions in some ceramics [20,53–55]. With decrease of bond valence, the cation bond strength decrease, which in turn increase the restoring force for recovering the degree of distortion of octahedrons and consequently decrease the τ_f [20,53]. The tendency of τ_f values was consistent with the sum of cation bond valence (see Fig. 5d), which was according to the expression given above. It's worth mentioning that all the ceramics sintered at 1100–1140 °C exhibited near-zero τ_f values and the minimum τ_f value of +4.52 ppm/°C could be obtained at 1120 °C.

4. Conclusions

Olivine−structure microwave dielectric ceramics $LiYbSiO_4$ with near-zero τ_f were fabricated by solid-state reaction process for the first time. The variation in ε_r could be correlated with the Raman shift and the polarization of Yb^{3+} in the octahedrons. The variation in the $Q\times f$ values was inversely correlated to FWMH and the average cation covalency. The smaller sum of bond valence of cations represented the smaller τ_f values in this work. Single phase $LiYbSiO_4$ ceramics sintered at 1120 °C for 6h showed excellent microwave dielectric properties with ε_r = 7.42, $Q\times f$ = 25276 GHz and τ_f = +4.52 ppm/°C.

Declaration of competing interest

We declare that we have no financial and personal relationships with other people or organizations that can inappropriately influence our work. There is no professional or other personal interest in any product, service or company.

Acknowledgments

This work was supported by Natural Science Foundation of China (Nos. 21965009 and 21761008), the Natural Science Foundation of Guangxi Zhuang Autonomous Region (Nos. 2018GXNSFBA281093 and 2018GXNSFAA138175), and Projects of Department of Science and Technology of Guangxi (Nos. AA18118008, AA18118034 and AA18118023) and High level innovation team and outstanding scholar program of Guangxi institutes and Innovation Project of Guangxi Graduate Education (No. YCBZ2020066).

References

[1] M.I. Khattak, A. Sohail, U. Khan, Z. Barki, G. Witjaksono, Elliptical slot circular patch antenna array with dual band behaviour for future 5G mobile communication networks, Prog. Electromagnet. Res. C 89 (2019) 133–147.
[2] C.F. Xing, B. Wu, J. Bao, H.T. Wu, Y.Y. Zhou, Crystal structure, infrared spectra and microwave dielectric properties of a novel low-firing $Gd_2Zr_3(MoO_4)_9$ ceramic, Ceram. Int. 45 (2019) 22207–22214.
[3] X.Q. Song, W. Lei, Y.Y. Zhou, T. Chen, S.W. Ta, Z.X. Fu, W.Z. Lu, Ultra-low fired fluoride composite microwave dielectric ceramics and their application for $BaCuSi_2O_6$-based LTCC, J. Am. Ceram. Soc. 103 (2020) 1140–1148.
[4] H.H. Guo, D. Zhou, C. Du, P.J. Wang, W.F. Liu, L.X. Pang, Q.P. Wang, J.Z. Su, C. Singh, S. Trukhanov, Temperature stable $Li_2Ti_{0.75}(Mg_{1/3}Nb_{2/3})_{0.25}O_3$-based microwave dielectric ceramics with low sintering temperature and ultra-low dielectric loss for dielectric resonator antenna applications, J. Mater. Chem. C (2020), https://doi.org/10.1039/D0TC00326C.
[5] K.X. Song, P. Liu, H.X. Lin, W.T. Su, J. Jiang, S. Wu, J. Wu, Z.H. Ying, H.B. Qin, Symmetry of hexagonal ring and microwave dielectric properties of $(Mg_{1-x}Ln_x)_2Al_4Si_5O_{18+x}$ (Ln = La, Sm) cordierite-type ceramics, J. Eur. Ceram. Soc. 36 (2016) 1167–1175.
[6] G. Dou, D.X. Zhou, S.P. Gong, M. Guo, Low temperature sintering and microwave dielectric properties of Li_2ZnSiO_4 ceramics with ZB glass, J. Mater. Sci. Mater. Electron. 24 (2013) 1601–1607.
[7] H. Ohsato, T. Tsunooka, T. Sugiyama, et al., Forsterite ceramics for millimeterwave dielectrics, J. Electroceram. 17 (2006) 445–450.
[8] H. Sun, Q. Zhang, H. Yang, J. Zou, $(Ca_{1-x}Mg_x)SiO_3$: a low-permittivity microwave dielectric ceramic system, Mater. Sci. Eng. B. Solid-State Mater. Adv. Technol. 138 (2007) 46–50.
[9] Y. Guo, H. Ohsato, K.I. Kakimoto, Characterization and dielectric behavior of willemite and TiO_2-doped willemite ceramics at millimeter-wave frequency, J. Eur. Ceram. Soc. 26 (2006) 1827–1830.
[10] H.B. Barzegar, B. Liu, W.T. Su, K.X. Song, $Ca_3MgSi_2O_8$: novel low-permittivity microwave dielectric ceramics for 5G application, Mater. Lett. 263 (2020) 127248, https://doi.org/10.1016/j.matlet.2019.127248.
[11] A. Sunny, K.A. Lazer, K.M. Manu, K.P. Surendran, M.T. Sebastian, Effect of glass fluxing on densification and microwave dielectric properties of $LiInSiO_4$ ceramic, J. Alloys Compd. 552 (2013) 83–87.
[12] C. Jiang, S.P. Wu, Q. Ma, Y.X. Mei, Synthesis and microwave dielectric properties of Nd_2SiO_5 ceramics, J. Alloys Compd. 544 (2012) 141–144.
[13] W. Lei, R. Ang, X.C. Wang, W.Z. Lu, Phase evolution and near-zero shrinkage in $BaAl_2Si_2O_8$ low-permittivity microwave dielectric ceramics, Mater. Res. Bull. 50 (2014) 235–239.
[14] K. Du, Z.Y. Zou, X.Q. Song, J. Fan, W.Z. Lu, W. Lei, Correlation between crystal structure and microwave dielectric properties of $CaRE_4Si_3O_{13}$ (RE = La, Nd, Sm, and Er), J. Mater. Sci. Mater. Electron. 31 (2020) 3274–3280.
[15] K.M. Manu, T. Joseph, M.T. Sebastian, Temperature compensated $Sr_2Al_2SiO_7$ ceramic for microwave applications, Mater. Chem. Phys. 133 (2012) 21–23.
[16] M. Terada, K. Kawamura, I. Kagomiya, K.I. Kakimoto, H. Ohsato, Effect of Ni substitution on the microwave dielectric properties of cordierite, J. Eur. Ceram. Soc. 27 (2007) 3045–3048.
[17] Q.B. Lin, K.X. Song, B. Liu, H.B. Bafrooei, D. Zhou, W.T. Su, F. Shi, D.W. Wang, H.X. Lin, I.M. Reaney, Vibrational spectroscopy and microwave dielectric properties of $AY_2Si_3O_{10}$ (A = Sr, Ba) ceramics for 5G applications, Ceram. Int. 46 (2020) 1171–1177.
[18] I.J. Induja, M.T. Sebastian, Microwave dielectric properties of mineral sillimanite obtained by conventional and cold sintering process, J. Eur. Ceram. Soc. 37 (2017) 2143–2147.
[19] S. Thomas, M.T. Sebastian, Microwave dielectric properties of $SrRE_4Si_3O_{13}$ (RE = La, Pr, Nd, Sm, Eu, Gd, Tb, Dy, Er, Tm, Yb, and Y) ceramics, J. Am. Ceram. Soc. 92 (2009) 2975–2981.
[20] K.M. Manu, C. Karthik, L.C. Leu, K.A. Lazar, R. Ubic, M.T. Sebastian, Crystal structure and microwave dielectric properties of $LiRE_9(SiO_4)_6O_2$ ceramics (RE = La, Pr, Nd, Sm, Eu, Gd, and Er), J. Am. Ceram. Soc. 96 (2013) 1504–1511.
[21] S.H. Kweon, M.R. Joung, J.S. Kim, B.Y. Kim, S. Nahm, J.H. Paik, Y.S. Kim, T.H. Sung, Low temperature sintering and microwave dielectric properties of B_2O_3-added $LiAlSiO_4$ ceramics, J. Am. Ceram. Soc. 94 (2011) 1995–1998.
[22] S.P. Wu, D.F. Chen, C. Jiang, Y.X. Mei, Q. Ma, Synthesis of monoclinic $CaSnSiO_5$ ceramics and their microwave dielectric properties, Mater. Lett. 91 (2013) 239–241.
[23] J.S. Wei, Z.H. Xu, P. Liu, W.T. Su, H.X. Lin, P. Zheng, J.M. Xu, K.X. Song, H.B. Q, $Ba_9Y_2Si_6O_{24}$: a new silicate dielectric ceramic for microwave communication application, Mater. Lett. 178 (2016) 144–146.
[24] K. Cheng, Y. Tang, H.C. Xiang, C.C. Li, L. Fang, Y.H. Sun, Two novel low permittivity microwave dielectric ceramics Li_2TiMO_5 (M = Ge, Si) with abnormally positive τ_f, J. Eur. Ceram. Soc. 39 (2019) 2680–2684.
[25] M.T. Paques-Ledent, P. TarteVibrational, Studies of olivine-type compounds—II. Orthosilicates, -arsenates and –vanadates $A^IB^{II}X^VO_4$, Spectrochim. Acta A. 30 (1974) 678–679.
[26] D. Thomas, M.T. Sebastian, Temperature-compensated $LiMgPO_4$: a new glass-free low-temperature cofired ceramic, J. Am. Ceram. Soc. 93 (2010) 3828–3831.
[27] P. Zhang, S.X. Wu, M. Xiao, The microwave dielectric properties and crystal structure of low temperature sintering $LiNiPO_4$ ceramics, J. Eur. Ceram. Soc. 38 (2018) 4433–4439.
[28] X. Hu, Z.F. Cheng, Y. Li, Z.Y. Ling, Dielectric relaxation and microwave dielectric properties of low temperature sintering $LiMnPO_4$ ceramics, J. Alloys Compd. 651 (2015) 290–293.
[29] E.C. Xiao, Z.K. Cao, J.Z. Li, X.H. Li, M.T. Liu, Z.X. Yue, Y. Chen, G.H. Chen, K.X. Song, H.F. Zhou, F. Shi, Crystal structure, dielectric properties, and lattice vibrational characteristics of $LiNiPO_4$ ceramics sintered at different temperatures, J. Am. Ceram. Soc. 103 (2020) 2528–2539.
[30] K. Cheng, C.C. Li, H.C. Xiang, Y.H. Sun, L. Fang, $LiYGeO_4$: novel low-permittivity microwave dielectric ceramics with intrinsic low sintering temperature, Mater. Lett. 228 (2018) 96–99.
[31] S. Nakayama, M. Sakamoto, Microstructures and electrical properties for $LiXSiO_4$ (X = Al, Y, La, Nd, Sm, Gd, Dy, Ho, Er, Yb), J. Ceram. Soc. Jpn. 100 (1992) 867–871.
[32] M. Nakayama, M. Kimura, R. Jalem, T. Kasuga, Efficient automatic screening for Li ion conductive inorganic oxides with bond valence pathway models and percolation algorithm, Jpn. J. Appl. Phys. 55 (1S) (2016) 01AH05.
[33] R.J. Xiao, H. Li, L.Q. Chen, Candidate structures for inorganic lithium solid-state

electrolytes identified by high-throughput bond-valence calculations, J. Materiomics 1 (2015) 325–332.
[34] L.A. Khalam, H. Sreemoolanathan, R. Rathees, P. Mohanan, M.T. Sebastian, Preparation, characterization and microwave dielectric properties of $Ba(B'_{1/2}Nb_{1/2})O_3$ [B′= La, Pr, Nd, Sm, Eu, Gd, Tb, Dy, Ho, Y, Yb and In] ceramics, Mater. Sci. Eng. B 107 (2004) 264–270.
[35] C.F. Tseng, Microwave dielectric properties of a new $Cu_{0.5}Ti_{0.5}NbO_4$ ceramics, J. Eur. Ceram. Soc. 35 (2015) 383–387.
[36] V.N. Morris, R.A. Farrell, A.M. Sexton, M.A. Morris, Lattice constant dependence on particle size for bulk and doped ceria prepared from a citrate sol–gel, J. Phys. Conf. Ser. 26 (2006) 119–122.
[37] H.F. Zhou, J.Z. Gong, G.C. Fan, X.L. Chen, Enhanced sintering ability and microwave dielectric properties of $LiZnNbO_4$ ceramics with pretreatment of raw materials, J. Alloys Compd. 665 (2016) 113–118.
[38] C.J. Pei, C.D. Hou, Y. Li, G.G. Yao, Z.Y. Ren, P. Liu, H.W. Zhang, A low ε_r and temperature-stable $Li_3Mg_2SbO_6$ microwave dielectric ceramics, J. Alloys Compd. 792 (2019) 46–49.
[39] C. Zhang, R.Z. Zuo, J. Zhang, Y. Wang, Structure-dependent microwave dielectric properties and middle-temperature sintering of forsterite $(Mg_{1-x}Ni_x)_2SiO_4$ ceramics, J. Am. Ceram. Soc. 98 (2015) 702–710.
[40] R. Peng, Y.X. Li, X.L. Tang, Y.C. Lu, Q. Zhang, X.Y. Wang, H. Su, Improved sintering and microwave dielectric properties of Li_2CaSiO_4 ceramic with magnesium atom substitution, Ceram. Int. 46 (2019) 8869–8876.
[41] M.T. Paques-Ledent, Vibrational studies of olivine-type compounds—III. orthosilicates and germanates $A^IB^{III}X^{IV}O_4$, Spectrochim. Acta A. 32 (1976) 383–395.
[42] C.A. Geiger, B.A. Kolesov, Microscopic-macroscopic relationships in silicates: examples from IR and Raman spectroscopy and heat capacity measurements, in: C.M. Gramaccioli (Ed.), EMU Notes in Mineralogy, Budapest, 2002, pp. 347–387.
[43] Q. Liao, L.X. Li, Structural dependence of microwave dielectric properties of ixiolite structured $ZnTiNb_2O_8$ materials: crystal structure refinement and Raman spectra study, Dalton Trans. 41 (2012) 6963–6969.
[44] T.L. Sun, X.M. Chen, Raman spectra analysis for $Ba[(Mg_{1-x}Ni_x)_{1/3}Nb_{2/3}]O_3$ microwave dielectric ceramics, AIP. Adv. 5 (2015) 17106, https://doi.org/10.1063/1.4905740.
[45] I.D. Brown, R.D. Shannon, Empirical bond-strength-bond-length curves for oxides, Acta Crystallogr. A. 29 (1973) 266–282.
[46] A.J. Bosman, E.E. Havinga, Temperature dependence of dielectric constants of cubic ionic compounds, Phys. Rev. 129 (1963) 1593–1600.
[47] R.D. Shannon, Dielectric polarizabilities of ions in oxides and fluorides, J. Appl. Phys. 73 (1993) 348–366.
[48] R.D. Shannon, G.R. Rossman, Dielectric constants of silicate garnets and the oxide additivity rule, Am. Mineral. 77 (1992) 94–100.
[49] Y. Lai, H. Su, G. Wang, X. Tang, X. Liang, X. Huang, Improved microwave dielectric properties of $CaMgSi_2O_6$ ceramics through CuO doping, J. Alloys Compd. 772 (2019) 40–48.
[50] J. Varghese, T. Siponkoski, M. Nelo, M.T. Sebastian, H. Jantunen, Microwave dielectric properties of low-temperature sinterable α-MoO_3, J. Eur. Ceram. Soc. 38 (2018) 1541–1547.
[51] N. Joseph, J. Varghese, T. Siponkoski, M. Teirikangas, M.T. Sebastian, H. Jantunen, Glass-free $CuMoO_4$ ceramic with excellent dielectric and thermal properties for ultralow temperature cofired ceramic applications, ACS Sustain. Chem. Eng. 4 (2016) 5632–5639.
[52] B. Li, L. Qiu, H.S. Leng, Effect of Mg^{2+} substitution on the crystal structure and microwave dielectric properties of $Ca_5Mn_4(VO_4)_6$ ceramics, Mater. Res. Bull. 118 (2019) 110510, https://doi.org/10.1016/j.materresbull.2019.110510.
[53] S.D.R. Rao, S.R. Kiran, V.R.K. Murthy, Correlation between structural characteristics and microwave dielectric properties of scheelite $Ca_{1-x}Cd_xMoO_4$ solid solution, J. Am. Ceram. Soc. 95 (2012) 3532–3537.
[54] M.W. Lufaso, Crystal structures, modeling, and dielectric property relationships of 2:1 ordered $Ba_3MM'_2O_9$ (M = Mg, Ni, Zn; M'= Nb, Ta) perovskites, Chem. Mater. 16 (2004) 2148–2156.
[55] Y.M. Lai, X.L. Tang, X. Huang, H.W. Zhang, X.F. Liang, J. Li, H. Su, Phase composition, crystal structure and microwave dielectric properties of $Mg_{2-x}Cu_xSiO_4$ ceramics, J. Eur. Ceram. Soc. 38 (2018) 1508–1516.
[56] H.L. Pan, C.F. Xing, J.X. Bi, X.S. Jiang, Y.X. Mao, H.T. Wu, Sintering characteristics and microwave dielectric properties of low loss $MgZrNb_2O_8$ ceramics achieved by reaction sintering process, J. Alloys Compd. 687 (2016) 274–279.